Ecosystems
https://doi.org/10.1007/s10021-020-00584-7

Divergent Controls on Stream Greenhouse Gas Concentrations Across a Land-Use Gradient

Allison M. Herreid,[1]* Adam S. Wymore,[1] Ruth K. Varner,[2] Jody D. Potter,[1] and William H. McDowell[1]

[1]*Department of Natural Resources and the Environment, University of New Hampshire, 56 College Road, Durham, New Hampshire, USA;* [2]*Institute for the Study of Earth, Oceans and Space and Department of Earth Sciences, University of New Hampshire, 8 College Road, Durham, New Hampshire, USA*

Abstract

Inland waters can be significant sources of carbon dioxide (CO_2), methane (CH_4) and nitrous oxide (N_2O) to the atmosphere. However, considerable uncertainty remains in regional and global estimates of greenhouse gas (GHG) emissions from freshwater ecosystems, particularly streams. Controls on GHG production in streams, such as water chemistry and sediment characteristics, are also poorly understood. The main objective of this study was to quantify spatial and temporal variability in GHG concentrations in 20 streams across a landscape with considerable variation in land use and land cover in New England, USA. Stream water was consistently supersaturated in CO_2, CH_4, and N_2O, suggesting that these small streams are sources of GHGs to the atmosphere in this landscape. Results show that concentrations of dissolved CO_2, CH_4 and N_2O differed in their spatial and temporal patterns and in their relationship to stream chemistry. Both bivariate and multivariate analyses revealed a unique combination of predictor variables for each gas, suggesting variation in the landscape attributes and in-stream processes that control GHG concentrations. Although hydrologic conditions did not explain variation among sites, temporal patterns in GHG concentrations align with seasonal phenologies in flow and temperature. We developed a conceptual model based on these data that describes the spatial variability in GHG production from streams and that can elucidate the dominant controls on each gas. Developing an understanding of the factors controlling GHG dynamics in streams can help assess and predict how fluvial ecosystems will respond to changes in climate and land use and can be used to incorporate emissions from streams into regional and global GHG emission inventories.

Key words: Carbon dioxide; Nitrous oxide; Methane; Streams; Greenhouse gas; Sediment.

Received 10 August 2020; accepted 27 October 2020

Electronic supplementary material: The online version of this article (https://doi.org/10.1007/s10021-020-00584-7) contains supplementary material, which is available to authorized users.

Author Contributions A.H. designed the study with input from A.S.W., R.K.V., J.D.P. and W.H.M. A.H. performed research, field work, and all sample and data analyses. A.H. wrote the paper with suggestions from A.S.W., R.K.V., J.D.P. and W.H.M.. All authors revised manuscript prior to submission.

**Corresponding author; e-mail:* ah1208@wildcats.unh.edu

Published online: 02 December 2020

Highlights

- Stream CO_2, CH_4 and N_2O concentrations differ in their spatial and temporal patterns.
- N_2O concentrations are influenced by water chemistry and land use.
- Hyporheic conditions are particularly important in controlling CH_4 concentrations.

Introduction

Freshwater ecosystems can be important sources of greenhouse gases (GHGs) to the atmosphere due to their ability to actively process and transform terrestrial inputs of organic matter and other solutes (Cole and others 2007; Battin and others 2009). Although the terrestrial landscape is generally considered a carbon (C) sink, with recent estimates suggesting a net uptake of 3.6 Pg C per year (Keenan and Williams 2018), streams and rivers may provide sufficient emissions of GHGs to offset the terrestrial C sink. Streams are frequently supersaturated not only in carbon dioxide (CO_2), but also in methane (CH_4) (Bastviken and others 2011; Stanley and others 2016) and nitrous oxide (N_2O) (Wilcock and Sorrell 2008; Baulch and others 2011; Beaulieu and others 2011; Schade and others 2016; Audet and others 2017).

Although streams are sources of all three greenhouse gases, recent flux estimates are largely focused only on the outgassing of CO_2. One of the first estimates of outgassing of C from fluvial ecosystems by Cole and others (2007) was an admittedly conservative 0.8 Pg C per year. Over the following decade, this estimate was revised upward to 1.8 Pg C per year (Raymond and others 2013) and then again to 3.9 Pg C per year (Drake and others 2018). Estimates of the total surface area of rivers and streams globally were also recently increased (Allen and Pavelsky 2018). Collectively, these new estimates highlight the importance of incorporating fluxes of GHGs from fluvial ecosystems in global carbon budgets. Although the magnitude of CH_4 and N_2O emissions is generally lower than that of CO_2, these gases are more effective at trapping heat (Myhre and others 2013) and thus aggregating GHG emissions from streams is critical to understanding the contribution of streams and rivers to atmospheric fluxes of GHGs.

To improve estimates of GHG emissions from fluvial ecosystems, it is important to develop a cohesive understanding of the multiple factors driving gas production and consumption. Distinguishing controls on GHGs is complex given the interactive nature of C and N cycling and the large number of biotic and abiotic factors that influence GHG concentrations. Broadly, CO_2 concentrations are controlled by the tradeoff between respiration and primary production, and the factors that fuel these processes (for example, oxygen (O_2) and organic C availability) (Cole and others 2007). Methane concentrations are strongly controlled by organic matter availability and redox conditions (Stanley and others 2016), and N_2O concentrations are tightly linked to the factors that influence N cycling processes [for example, O_2, nitrate (NO_3^-) availability] (Burgin and Hamilton 2007; Quick and others 2019). Various studies have investigated controls on GHGs in fluvial ecosystems but results to date are varied and often contradictory. For example, many studies have observed the expected relationship between NO_3^- and N_2O concentrations that have been invoked as evidence for both nitrification and denitrification controlling N_2O production (Harrison and Matson 2003; Baulch and others 2011; Beaulieu and others 2011; Schade and others 2016; Turner and others 2016; Audet and others 2017). In contrast, controls on CH_4 dynamics are more uncertain. In temperate forest streams organic C availability drives overall gas flux (that is all three gases), but concentrations of NO_3^- regulate the magnitude of N_2O and CH_4 production, with higher NO_3^- concentrations resulting in lower fluxes of CH_4 (Schade and others 2016). However, no effect of NO_3^- on concentrations and fluxes of CH_4 was found in predominantly agricultural streams with relatively high NO_3^- concentrations (Crawford and Stanley 2016). This suggests that drivers and inhibitors of CH_4 production may not be universal across systems, underscoring the need to untangle the complicated relationships between C and N cycling processes and GHG dynamics (Stanley and others 2016).

The objective of our study was to identify drivers of spatial and temporal variability in dissolved greenhouse gas concentrations in small temperate streams that drain watersheds in New Hampshire and Maine. Twenty study streams were selected across a land-use gradient to provide a range of water chemistry, and environmental and physical conditions. Developing an improved understanding of greenhouse gas dynamics in fluvial ecosystems will allow us to better incorporate streams and rivers into global emissions inventories and into biogeochemical models of GHG production and emission.

Methods

Study Area

The twenty streams chosen for study came from a database of streams within the Great Bay watershed, in southeastern New Hampshire and southwestern Maine, USA, compiled by the Water Quality Analysis Lab (WQAL) of the University of New Hampshire (UNH) (Figure 1). Using previously collected water quality data, we selected low-order streams (mean watershed area = 2.82 km^2) along a gradient of NO_3 concentrations. The twenty study streams encompass a wide range of land use and land cover, allowing us to test controls on the spatial and temporal heterogeneity of GHGs. Our study includes sites dominated by forest (up to 99% cover), wetlands (up to 34% cover), agriculture (up to 51% cover), or urban development (up to 54% cover) resulting in a range of concentrations of dissolved inorganic nitrogen (0.04–1.37 mg N L^{-1} as NO_3^-; 10.9–286 µg L^{-1} as NH_4^+, Table 1).

Water Chemistry and Dissolved Gas Collection

We collected surface water samples monthly at each stream for one year. Samples were collected from the thalweg of each stream during daylight hours. Water chemistry samples were collected in acid-washed syringes and field filtered through pre-combusted glass fiber filters (0.7 µm; Whatman GF/F) into 60-mL acid-washed HDPE bottles and amber vials and stored in a cooler with ice until being returned to the laboratory that same day. Samples were then frozen or refrigerated for subsequent analysis. Dissolved gas samples were collected in triplicate at each stream using acid-washed 60-mL polypropylene syringes fitted with two-way stopcocks. Syringes were filled to 30 mL with stream water, cleared of air bubbles, and emptied and refilled to 30 mL underwater (again clearing air bubbles). Syringes were kept on ice and returned to the WQAL within eight hours of collection. Hand-held measurements of dissolved oxygen (DO, percent saturation and concentration in mg L^{-1}), specific conductance (µS cm^{-1}), pH, and water temperature (°C) were recorded at the time of collection using a YSI multiparameter probe (YSI ProDSS, Yellow Spring, OH).

Water Chemistry Analysis

We analyzed each sample for concentrations of NO_3^-, ammonium (NH_4^+), total dissolved nitrogen (TDN), dissolved organic carbon (DOC), soluble reactive phosphorus (SRP), dissolved organic matter (DOM) optical properties, and major cations (magnesium (Mg^{2+}), calcium (Ca^{2+}), potassium

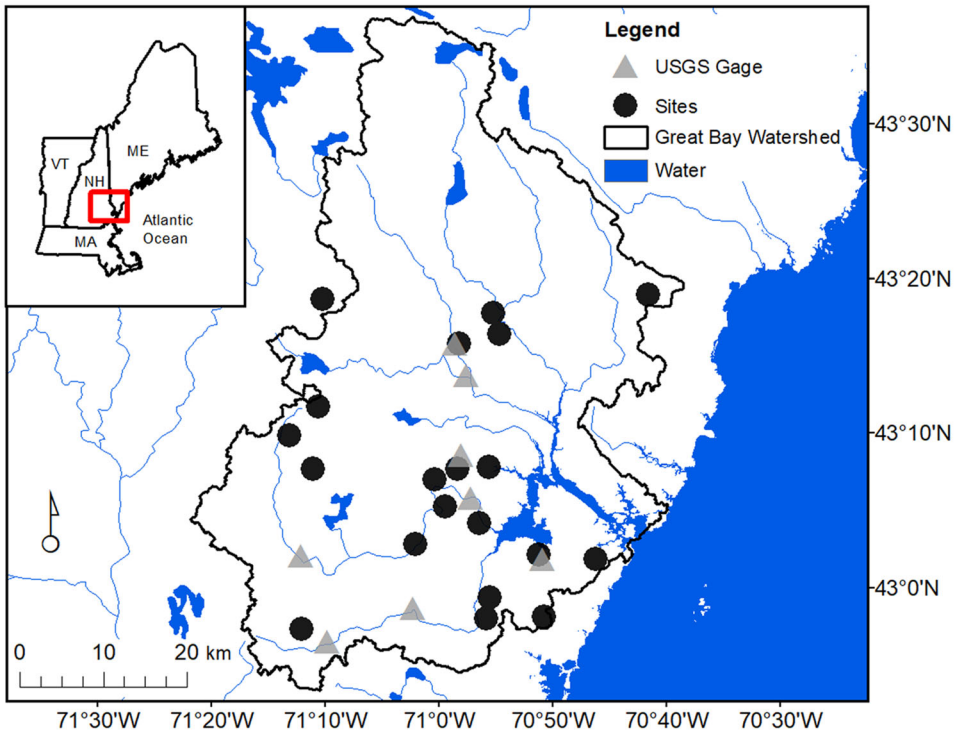

Figure 1. Map of Study Streams and USGS Gages Located in Southeastern New Hampshire and Southern Maine.

Table 1. Stream and Watershed Characteristics Across the 20 Study Sites Over Time.

	Mean	Minimum	Maximum
NO_3^- (mg N L^{-1})	0.51	0.04	1.37
DOC (mg C L^{-1})	6.68	1.68	16.30
TDN (mg N L^{-1})	0.79	0.08	1.97
NH_4^+ (µg N L^{-1})	44	11	286
DON (mg N L^{-1})	0.24	0.00	0.51
Cl^- (mg Cl L^{-1})	91.41	3.36	224.3
SO_4^{2-} (mg S L^{-1})	2.71	0.66	4.42
Acetate (mg L^{-1})	0.12	0.07	0.18
PO_4^{3-} (µg P L^{-1})	15	4	125
Na^+ (mg Na L^{-1})	55.07	2.12	146.3
K^+ (mg K L^{-1})	2.81	0.17	8.85
Mg^{2+} (mg Mg L^{-1})	4.13	0.026	8.02
Ca^{2+} (mg Ca L^{-1})	18.65	1.39	45.40
pH	6.7	4.9	7.4
Specific conductance (µs cm^{-1})	395.7	19.2	930.8
Dissolved O_2 (% saturation)	85.0	65.0	96.6
Temperature (°C)	8.89	7.36	10.33
SUVA	4.00	3.29	4.72
FI	1.36	1.27	1.49
HIX	0.90	0.76	0.96
Slope ratio	0.86	0.77	1.16
% developed	21%	0%	54%
% agriculture	12%	0%	51%
% forest	54%	31%	99%
% wetland	7%	0%	34%
% impervious	17%	1%	33%
Depth to refusal (cm)	11.0	0.0	38.0
Sediment %C	1.0%	0.2%	5.6%
Sediment %N	0.1%	0.0%	0.3%
Sediment C:N	18.3	2.1	38.8

Each metric was first averaged across site.

(K^+), and sodium (Na^+) and anions [chloride (Cl^-), sulfate (SO_4^{2-}), and acetate (CH_3COO^-)]. Samples were analyzed for TDN and DOC using high-temperature catalytic oxidation (Shimadzu TOC-L with a TNM-1 nitrogen analyzer), for NO_3^- and major anions and cations using ion chromatography with suppressed conductivity detection (Anions/Cations Dionex ICS-1000), for NH_4^+ using automated colorimetry (Unity Scientific SmartChem 200 discrete analyzer), and for SRP using automated colorimetry (Seal Analytical AQ2 discrete analyzer). Dissolved organic nitrogen (DON) concentrations were determined from the difference of TDN and dissolved inorganic nitrogen concentrations (DIN = NO_3^- + NH_4^+). UV absorbance was measured using HPLC with a photo-diode array detector (Shimadzu SPD-20A) that scanned from 200 to 700 nm in 1-nm intervals. The absorbance at wavelength of 254 nm was used to determine specific ultra-violet absorbance (SUVA, L mg-C^{-1} m^{-1}) following established methods (Weishaar and others 2003). Humification index (HIX) was determined as the ratio between the area under the 435–480 nm emission spectra peak and the sum of the peak areas between 330–345 and 435–490 nm (Ohno 2002). Fluorescence index (FI) was determined as the ratio of 470–520 nm fluorescence intensities at an excitation of 370 nm and used to identify sources (allochthonous vs. autochthonous) of DOM (McKnight and others 2001). Log transformed absorption spectra in the ranges of 275–295 and 350–400 nm were fit nonlinearly to an exponential function to determine spectral slope (S) (Helms and others 2008). Slope ratio (S_R) was calculated as the ratio of slopes for the 275–295 and 350–400 nm ranges. Slope ratio provides insights into molecular weight and aromaticity of DOM (Helms and others 2008). Analyses were conducted at the WQAL at UNH.

Dissolved Gas Analysis

Within 8 h of sample collection, 30 mL of helium was introduced to each sample. Syringes were then shaken for 5 min to equilibrate gases between the water and headspace (Mulholland and others 2004). The 30-mL equilibrated head space of each syringe was then injected into 20-mL evacuated, airtight vials. Gas samples were analyzed for concentrations of CO_2, CH_4, and N_2O using a Shimadzu GC-2014 gas chromatograph. A thermal conductivity detector (TCD) was used to detect CO_2, a flame ionization detector (FID) to detect CH_4, and an electron capture detector (ECD) to detect N_2O. Standards of CO_2 (1.8% error), CH_4 (1.7% error), and N_2O (2.2% error) are analyzed at the beginning of each run and after every 12 samples. Headspace gas concentrations (in ppmv) were converted to the concentration of dissolved gas in the initial water sample (in μM) accounting for the Bunsen solubility coefficients of each gas (Mulholland and others 2004) using temperature and atmospheric pressure of the head space equilibration.

Percentage saturation of each gas sample was calculated as:

$$\%\text{sat} = \frac{\text{Conc}_{\text{obs}}}{\text{Conc}_{\text{eq}}} * 100 \quad (1)$$

where Conc_{obs} is measured concentration of dissolved gas in the stream and Conc_{eq} is the expected concentration of each gas if the stream water was in equilibrium with the atmosphere (Audet and others 2017). Equilibrium concentrations were calculated using stream temperature and atmospheric pressure at the time of sample collection and Bunsen solubility coefficients of each gas. If atmospheric pressure was not recorded at the time of sampling, we used data from one site (WHB01) with continuous atmospheric pressure readings at 5-minute intervals and corrected by elevation for each site.

Porewater Samples

At a subset of sites (n = 9) we collected sediment porewater and gas samples using a porewater extracting device. Although we attempted porewater collection at all sites, many have cobble or gravel streambeds with little to no sediment, making porewater collection impossible. The porewater sampler is made of 3.175 mm o.d. stainless steel tubing with fine holes at the sampling end that allows porewater to enter the sampler (Noyce and others 2014). The top of the sampler is fitted with a two-way stopcock. The sampling end of the device was inserted into the sediment to the point of refusal (and at multiple depths in sites with deep sediments), and porewater samples were extracted using a syringe. Porewater samples were collected by attaching an acid-washed 60-mL syringe to the two-way stopcock and pulling the syringe plunger to extract the sample. Samples were analyzed for the same analytes as the surface water and dissolved gas samples.

Sediment Analyses

Channel and sediment attributes were characterized once during the duration of the study at the main sampling location, and at an additional cross-section 5–10 m upstream from the main location. Estimates of the depth of fine sediments overlying the coarse layer were made by measuring depth to refusal (Lisle and Hilton 1992). Five measurements were taken at each cross section. Sediment samples were collected at the primary sampling location and at a location $\sim$ 20 m upstream. Sediment samples were dried at 60°C for several days. Dried samples were sieved (1 mm) to remove larger rocks and pebbles. Remaining sediment was finely ground using a mortar and pestle in preparation for elemental analysis. Samples were run for weight percent carbon and nitrogen using a PerkinElmer 2400 Series II CHNS/O analyzer. C/N ratios were determined using the mass of each element.

Hydrology

Recognizing the importance of hydrological controls on stream GHG concentrations (Dinsmore and others 2013b; Stanley and others 2016), we obtained daily discharge data from United States Geological Survey (USGS) gages in our study area (Table S1) as we were unable to measure discharge at all of our sites every month. We used data from the eight gages located in the Piscataqua River basin given their proximity to our sampling locations (Figure 1). Discharge data from each of our sampling dates were converted to runoff (mm day^{-1}) and averaged across the eight stations to create a hydrologic index for each sampling month.

Statistical Analyses

Data that exhibited high levels of skewness, kurtosis, and failed the Shapiro–Wilk tests for assumptions of normality were normalized using logarithmic or square root transformations. We ran Mantel tests for each gas to assess possible spatial

autocorrelation. To compare the relative magnitude of spatial and temporal variability for each gas, we calculated variance in GHG concentrations for each site and each sampling month and performed one-way analyses of variance between spatial and temporal variation. We assessed bivariate relationships between dissolved gas concentrations and metrics of stream chemistry using linear regression analysis with each sampling month at each stream treated as a separate data point. We used partial least squares (PLS) analysis to identify multivariate relationships between gas concentrations and predictor variables, given the ability for PLS to account for multicollinearity among predictor variables (Carrascal and others 2009). PLS provides variable importance on projection (VIP) scores that represent each variable's influence on the model. A VIP score threshold of 0.8 is generally recommended to identify those variables that exert strong influence on the model, with larger VIP scores having a greater influence on the model (Carrascal and others 2009). PLS models were created for CO_2, CH_4, and N_2O with all metrics of stream chemistry and land-use entered into the model (see Table 1). The top five predictor variables, as ranked by VIP score, were then used in linear mixed-effect models (LMMs) to assess how well these most influential variables predict gas concentrations when considered together while also accounting for repeated measures and heterogeneity among sites. A common concern with datasets like ours is the issue of lack of independence between samples that were collected from the same stream over time. Mixed-effect modeling is one approach that allows us to account for the hierarchical nature of the dataset and is increasingly being used to describe datasets with high spatial and temporal variability (Romić and others 2020; Santos and others 2019). Response variables CO_2, CH_4, and N_2O were analyzed separately as a function of the top five predictor variables for each respective gas as fixed effects, with site as a random effect. Linear mixed-effects models were created using the package lme4 in R (Bates and others 2015). Stepwise multiple regression was used to determine which of the top predictive factors, delineated through PLS VIP scores, significantly influenced measured gas concentrations. Variables from each model were excluded in a stepwise backward direction when the AIC values of the alternative models were lower. We used the MuMIn package (Barton 2019) to determine the amount of variance (R^2) explained by fixed effects alone (marginal, R^2_m) and together with the random effect (conditional, R^2_c) (Nakagawa and Schielzeth 2013). The level of significance for all analyses was 0.05. All statistical analyses were performed using the R software version 3.5.3 (R Development Core Team 2019).

Results

Water Chemistry and Dissolved Gases

The twenty study streams were variable in water chemistry and other watershed characteristics (Table 1). Streams ranged from nutrient-poor (0.04 mg NO_3-N L^{-1}) to relatively enriched (1.37 mg NO_3-N L^{-1}) and spanned a range of carbon availability (DOC 1.68–16.30 mg C L^{-1}; mean 6.7 mg C L^{-1}, Table 1). Optical properties of DOM, which provide insights into the composition of organic matter, generally showed a small range of variability across study streams (for example, FI range = 1.27–1.49; mean 1.36, Table 1). Sediment characteristics (depth of fine sediments and C and N content) were variable across study sites. Average depth to refusal was shallow, 11.0 cm (range = 0–38 cm) and average sediment C/N ratio was 18.3 (range = 2.1–38.8, Table 1).

Spatial variability was significantly greater than temporal variability for N_2O ($p < 0.001$), CH_4 ($p < 0.001$), and CO_2 ($p < 0.001$). Concentrations of dissolved gases were highly variable across our 20 sites. Dissolved CH_4 concentrations ranged from 0.01 to 13.5 µM (mean = 0.63 µM) across sites over the 12 sampling months, with dissolved N_2O concentrations ranging from 6.1 to 880 nM (mean = 55 nM), and dissolved CO_2 concentrations ranging from 41 to 651 µM (mean = 170 µM, Table 2). All streams were consistently supersaturated in all three gases (Table 2; Figure 2).

Carbon dioxide, N_2O, and CH_4 concentrations differed in their average temporal patterns and magnitude of variability (Figures 2, 3). Mean N_2O concentrations across sites peaked in January, followed by two spikes in late spring and fall consistent with periods of elevated NO_3^- concentrations (Figure 3a). Methane concentrations on average decreased in early spring and increased throughout late spring and summer as temperatures increased and flows generally decreased (Figure 3b, d). Average concentrations of CO_2 showed large peaks in January and during the summer (Figure 3c).

Drivers of Greenhouse Gas Concentrations

Results from the Mantel tests were insignificant for all three gases, suggesting that there was no relationship between geographic distance and gas

Table 2. Mean Dissolved Greenhouse Gas Concentrations and Percent Saturation (sat%) for Each Site.

Site	N_2O (nM)	N_2O sat (%)	CH_4 (μM)	CH_4 sat (%)	CO_2 (μM)	CO_2 sat (%)
BDC	399.6 (211.4)	2926 (1347)	0.26 (0.13)	7882 (5147)	223 (88)	1087 (322)
BNR	34.4 (6.7)	264 (83)	0.06 (0.04)	1555 (1100)	51 (5)	266 (83)
BRB	28.4 (13.4)	200 (77)	1.20 (0.87)	36,716 (27842)	348 (77)	1880 (746)
CSB02	144.8 (56.8)	1117 (587)	0.37 (0.25)	10,977 (9573)	295 (80)	1548 (755)
DCF03	16.0 (5.7)	114 (21)	0.22 (0.10)	7121 (4489)	81 (21)	433 (187)
FSB	26.6 (11.1)	195 (54)	0.16 (0.07)	4667 (2642)	104 (27)	555 (240)
GRBK	25.5 (12.0)	192 (69)	0.84 (0.56)	25,394 (17903)	210 (69)	1174 (492)
HVH	18.9 (3.8)	149 (52)	2.12 (3.87)	80,571 (162681)	191 (90)	1179 (970)
JMY	31.5 (6.7)	250 (73)	0.84 (0.57)	27,446 (22135)	243 (74)	1374 (731)
MLB01	38.7 (8.8)	305 (68)	2.40 (0.91)	68,816 (27418)	173 (33)	910 (313)
PB02.7	21.7 (6.3)	185 (58)	0.77 (0.26)	24,071 (11708)	116 (22)	659 (265)
PIK	28.6 (6.3)	218 (67)	1.63 (0.67)	46,129 (15261)	104 (19)	547 (145)
PKB	37.3 (24.1)	269 (202)	0.19 (0.09)	5932 (4187)	150 (44)	809 (403)
PST	46.0 (14.0)	344 (68)	0.67 (0.30)	19,319 (8919)	176 (51)	900 (223)
RMB04	20.1 (13.0)	146 (47)	0.28 (0.10)	8458 (3148)	102 (39)	563 (220)
SBM0.2	15.1 (7.2)	108 (29)	0.06 (0.05)	1611 (1543)	231 (196)	1382 (1408)
TPB	16.7 (7.3)	121 (33)	0.42 (0.22)	12,906 (8741)	95 (75)	493 (305)
TWB	93.4 (35.2)	765 (421)	0.24 (0.12)	7176 (4093)	159 (37)	875 (390)
WEB	18.5 (3.6)	151 (61)	0.81 (0.28)	24,070 (9554)	225 (62)	1270 (628)
WHB01	41.2 (17.1)	298 (97)	0.15 (0.10)	4781 (4256)	122 (109)	665 (684)
Mean	55.1	416%	0.68	21,280%	170	928%

Standard deviations in parentheses.

concentrations (N_2O $p = 0.91$; CH_4 $p = 0.47$; CO_2 $p = 0.28$). Simple linear regression analyses revealed significant relationships between both N_2O and CO_2 concentrations and individual solutes, but we found no significant bivariate relationships between any predictor variables and CH_4 concentrations. Across sites and time, DO and CO_2 concentrations showed a significant, negative relationship ($r^2 = 0.69$, $p < 0.0001$). Although saturation of DO and CO_2 varied spatially and temporally, DO was generally undersaturated, while CO_2 was supersaturated (Figure 4). Dissolved N_2O was positively related to concentrations of NO_3^- ($r^2 = 0.34$, $p < 0.0001$, Figure 5) and potassium (K^+) ($r^2 = 0.33$, $p < 0.0001$, Figure 6).

The partial least squares analysis for CO_2 identified 12 predictor variables with VIP scores of at least 0.8, with the top five being DO (% saturation), DOC and PO_4^{3-} concentrations, and percent wetland and forest (Table 3). The N_2O PLS model resulted in 13 predictor variables above the 0.8 threshold. The top five were percent agriculture, NO_3^- and K^+ concentrations, temperature, and percent forest (Table 3). Partial least squares analysis for CH_4 identified 14 predictor variables with the top five being percent agriculture, percent developed, NH_4^+ concentration, specific conductance, and percent forest (Table 3). For all linear mixed-effects models, site was an important factor when considering the influence of the fixed effects, as shown by the increase in the amount of variation explained (R_c^2) when including site as a random effect (Table 4). The results of the LMM for CO_2 indicate that four predictors (DO, DOC, PO_4^{3-}, and % Forest), in combination with site as a random effect, explain 77% of the variance. Carbon dioxide concentrations were positively related to DOC and negatively associated with DO%, % forest, and PO_4^{3-} concentrations (Table 4). Model results for N_2O identified that NO_3^-, K^+, temperature, and percent agriculture account for 88% of the variability in N_2O concentrations. Beta values indicate a positive influence of NO_3^- and K^+ concentrations and % agriculture, while temperature shows a negative relationship with N_2O concentrations (Table 4). Land use, % agriculture and % forest, and specific conductance accounted for 77% of the variance in CH_4 concentrations when site was included as a random effect. Both % agriculture and % forest were negatively related to CH_4 concentrations while specific conductance showed a slight positive relationship (Table 4).

Sediment Porewater

Across sites, CO_2 concentrations were consistently higher in the sediments (mean = 772 μM, range =

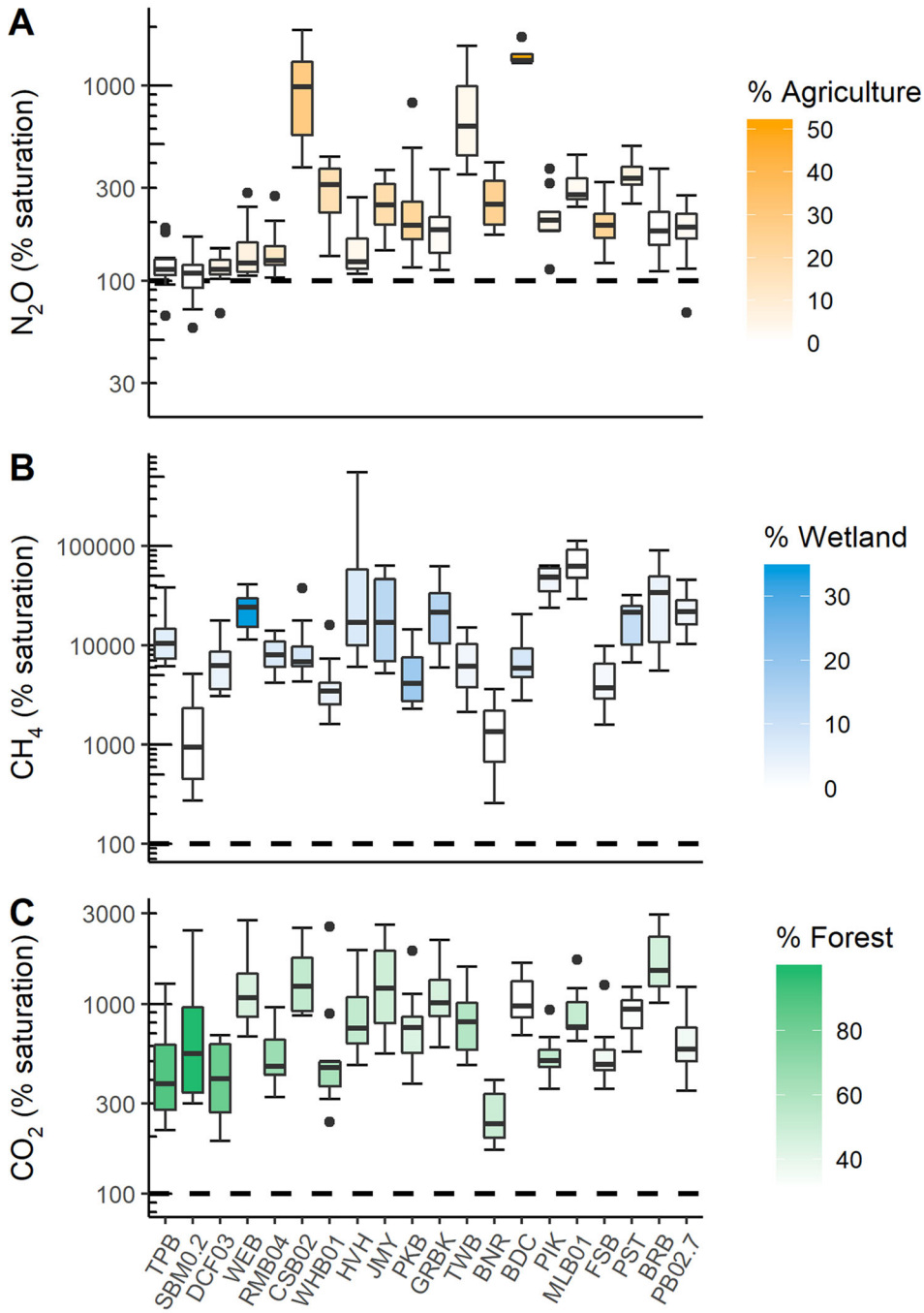

Figure 2. Boxplot panels representing percent saturation for N_2O (**A**), CH_4 (**B**), and CO_2 (**C**) across 12 months at 20 sites. Sites are ordered by increasing percent anthropogenic impact, defined as the sum of all anthropogenic land-cover types (% Agriculture, % Developed, % Impervious). Percent land cover shown to illustrate variation and range in land cover across sites. Note that the *y*-axis of each panel is presented in log scale.

69–3498 µM) than the surface water (mean = 133 µM, range = 41–310 µM), while N_2O concentrations were on average higher in the surface water (mean = 40 nM, range = 10–170 nM) than the sediments (mean = 30 nM, range = 10–210 nM). Methane concentrations were variable by site, with some having higher concentrations in the surface water (mean = 0.65 µM, range = 0.01–2.27 µM) and others having higher concentrations in the sediment porewater (mean = 32.07 µM, range = 0.01–325.03 µM).

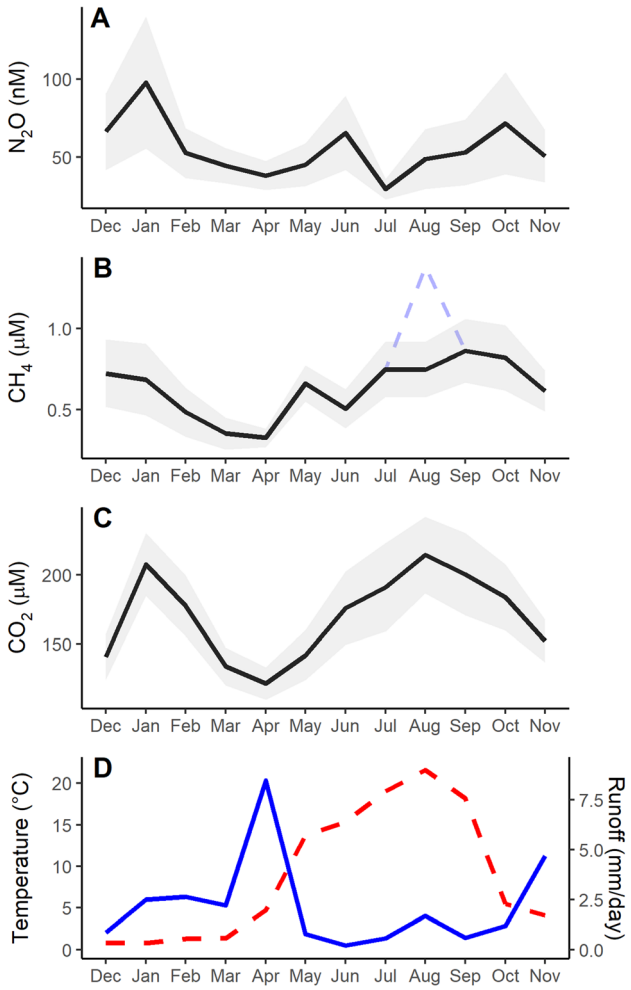

Figure 3. Mean N_2O (**A**), CH_4 (**B**), and CO_2 (**C**) concentrations across 20 sites over time. Panel (**D**) represents mean stream temperature (red) across sites over time and mean runoff from USGS gages in our study area (see Figure 1). The shaded ribbons represent standard error. On (**B**), the dashed blue line shows the seasonal pattern including the site HVH. See Figure S1 for temporal patterns for individual sites.

Surface water to porewater ratios for each gas allow us to compare the relative magnitude of differences in gas concentrations between the sediments and surface water. Ratios greater than one indicate higher concentrations in the surface water relative to the sediments, and those less than one indicate higher concentrations in the sediments. The mean ratio for CO_2 was 0.34 ± 0.29, 4.0 ± 5.3 for N_2O, and 4.7 ± 9.1 for CH_4 (Figure 7). Across sites, porewater CH_4 concentrations were positively correlated to the ratio of NH_4/NO_3 (Figure 8). A depth profile created for one site (PIK) shows a decline in N_2O, NO_3^-, and SO_4^{2-} with depth and a concomitant increase in CH_4 and NH_4^+ (Figure 9).

Discussion

Streams as Sources of GHGs

Each measured greenhouse gas exhibited unique spatial and temporal patterns, providing strong evidence that evasion losses are not the dominant driver of variability in dissolved gas concentrations. In assessing the relative magnitude of spatial and temporal variability in dissolved GHG concentrations, we found that all three gases showed significantly higher spatial than temporal variation. Although runoff did not appear as a strong predictor in our modeling approach, our temporal patterns suggest a close relationship between flow and GHG concentrations in this region, as shown by the association between high flows and low concentrations. Results confirm that streams are sources of greenhouse gases to the atmosphere, as

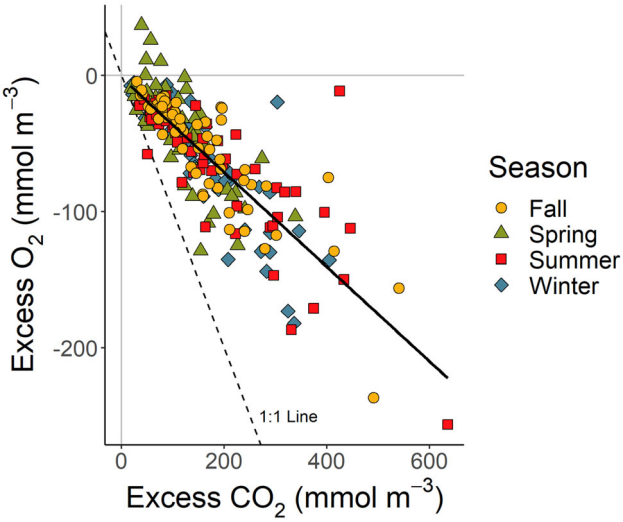

Figure 4. Relationship between dissolved CO_2 and O_2. Excess CO_2 or O_2 was calculated as the difference between measured concentrations and equilibrium concentrations expected if the stream water was in equilibrium with the atmosphere (that is, 100% saturation). The dashed 1:1 line represents the expected relationship between O_2 and CO_2 under the assumption that aerobic metabolism accounts for most of the measured CO_2 concentrations. The black line represents the linear regression between O_2 and CO_2 across sites and time ($r^2 = 0.69$, $p < 0.0001$).

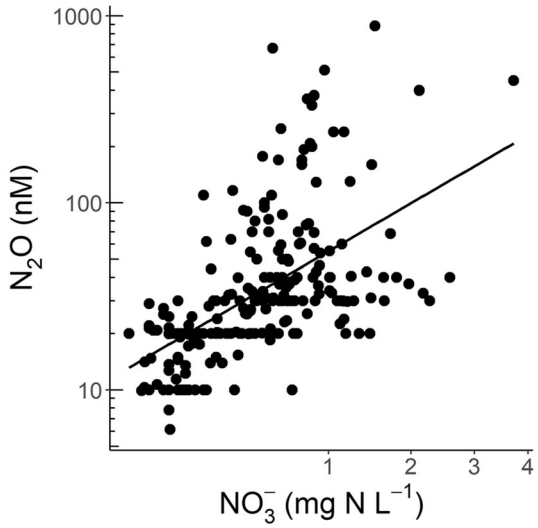

Figure 5. Linear regression between N_2O and NO_3^- concentrations across sites ($r^2 = 0.33$, $p < 0.0001$). Note that the *y*-axis is presented on a log scale and the *x*-axis is presented on a square root scale.

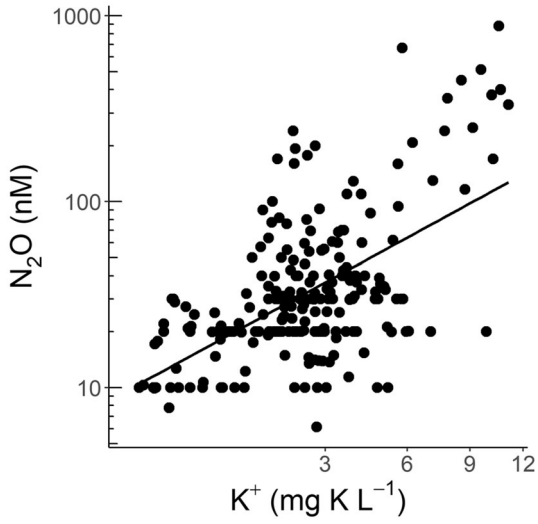

Figure 6. Linear regression between N_2O and K^+ concentrations across sites ($r^2 = 0.34$, $p < 0.0001$). Note that the *y*-axis is presented on a log scale and the *x*-axis is presented on a square root scale.

they are consistently supersaturated relative to atmospheric concentrations. Like previous studies (for example, Smith and others 2017), we found that no single, measured predictor variable was sufficient to explain variation in the concentrations of all three greenhouse gases. Although our results corroborate previous findings that N_2O production and concentrations correlate with NO_3^- concentrations (Baulch and others 2011; Beaulieu and others 2011), other factors (temperature, % agriculture, K^+ concentrations) provide additional explanatory power in characterizing temporal and spatial variability in N_2O concentrations. The results presented here support the growing body of literature suggesting that CH_4 concentrations are extremely variable in space and time and are highly dependent on local controls (Stanley and others 2016; Crawford and others 2017). The particularly strong vertical gradient we observed in CH_4 con-

Table 3. Variable Importance on Projection (VIP) Scores (≥ 0.8) of Predictor Variables for Carbon Dioxide (CO_2), Nitrous Oxide (N_2O), and Methane (CH_4) via Partial Least Squares (PLS) Analysis.

Predictor	N_2O	CH_4	CO_2
DO (%)	–	1.01	**2.90**[a]
DOC (mg C L^{-1})	–	0.87	**1.49**[a]
% Forest	**1.37**[a]	**1.33**[a]	**1.05**[a]
PO_4^{3-} (μg P L^{-1})	1.17	0.90	**1.04**[a]
% wetland	–	–	**1.04**[a]
pH	1.04	0.93	1.02
NH_4^+ (μg N L^{-1})	0.89	**1.49**[a]	1.01
FI	–	–	1.01
K^+ (mg K L^{-1})	**1.64**[a]	1.17	0.91
DON (mg N L^{-1})	–	–	0.86
SO_4^{2-} (mg S L^{-1})	1.19	1.07	0.85
HIX	–	–	0.83
DTR	–	–	–
% agriculture	**1.94**[a]	**1.90**[a]	–
Slope ratio	–	0.89	–
C:N	0.85	–	–
N	0.86	–	–
Runoff (mm day^{-1})	–	–	–
Temperature (C)	**1.36**[a]	0.87	–
NO_3^- (mg N L^{-1})	**1.73**[a]	0.90	–
% Developed	0.93	**1.76**[a]	–
Specific conductance	0.84	**1.48**[a]	–
SUVA	–	–	–
C	–	–	–

[a]*Bold-face denote top five VIP scores for each model (see Table 4).*
Dashes represent VIP scores < 0.8 for a given predictor variable. Higher VIP scores represent a greater influence on the model. Table is organized by CO_2 VIP scores.

centrations with depth in the stream sediments suggests that hyporheic conditions may be especially important in controlling CH_4 dynamics in stream water.

Our measured gas concentrations are comparable to previously reported values across ecosystems. Mean dissolved CO_2 concentrations (170 μM) and consistent supersaturation in our study streams (mean 928%) are similar to studies from the midwestern USA (Crawford and Stanley 2016), and higher than those reported for interior Alaska (Crawford and others 2013). Nitrous oxide concentrations in our study, which averaged 55 nM (416% saturation), were similar to those reported for streams draining agricultural landscapes in the midwestern USA (Beaulieu and others 2008) and slightly lower than for sites in an agricultural catchment in Sweden (Audet and others 2017). Although previous studies have shown that heavily impacted systems can be considerable sources of N_2O (Beaulieu and others 2008; Wilcock and Sorrell 2008; Baulch and others 2011; Audet and others 2017), our data provide evidence that even streams draining temperate and forested catchments with modest levels of agriculture (averaging 12% among our study watersheds) and relatively low concentrations of DIN (mean NO_3^- = 0.51 mg N L^{-1}) can produce considerable amounts of dissolved N_2O (Figure 2). Mean CH_4 concentrations in our 20 streams (0.68 μM) fall within the reported range of global CH_4 concentrations, though slightly less than the average (1.35 μM) (Stanley and oth-

Table 4. Results from Linear Mixed-Effects Models (LMMs) with Fixed Effects and the Random Effect of Site (not shown) for Dissolved Gas Concentrations.

Response	Fixed effects	β	R^2	
			R^2_m	R^2_c
N_2O (nM)	% agriculture	1.45	0.56	0.88
	NO_3^- (mg N L^{-1})	0.27		
	K^+ (mg K L^{-1})	0.05		
	Temperature (°C)	− 0.05		
CH_4 (μM)	% agriculture	− 2.03	0.33	0.77
	Specific conductance (μS cm^{-1})	0.01		
	% forest	− 1.34		
CO_2 (μM)	DO (%)	− 0.01	0.51	0.77
	DOC (mg C L^{-1})	0.07		
	% forest	− 0.31		
	PO_4^{3-} (μg P L^{-1})	− 0.05		

The fixed effects included in each initial model were selected based on the five highest variable importance on projection (VIP) scores as identified through partial least squares (see Table 3). Fixed effects that did not significantly improve the model were dropped through stepwise backward deletion based on AIC resulting in the final fixed effects displayed here. β values provide a measure of how strongly, and in which direction, each predictor influences the model. Marginal coefficient of determination (R_m^2) shows variation explained by fixed effects alone, while the conditional coefficient of determination (R_c^2) accounts for variation explained by both fixed and random effects.

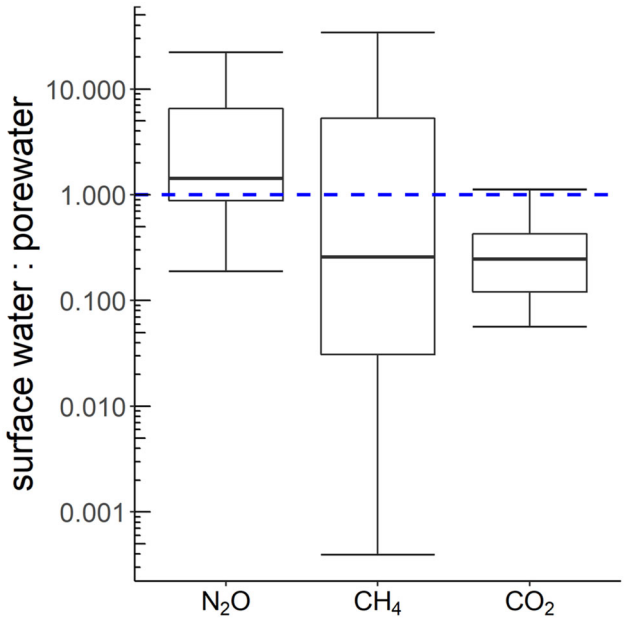

Figure 7. Ratio of surface water to porewater concentrations for each gas (n_{sites} = 9, for CO_2 and CH_4 $n_{samples}$ = 25, for N_2O $n_{samples}$ = 23). Values above one indicate gas concentrations are higher in the surface water relative to the porewater and values below one indicate higher concentrations in the sediment porewater.

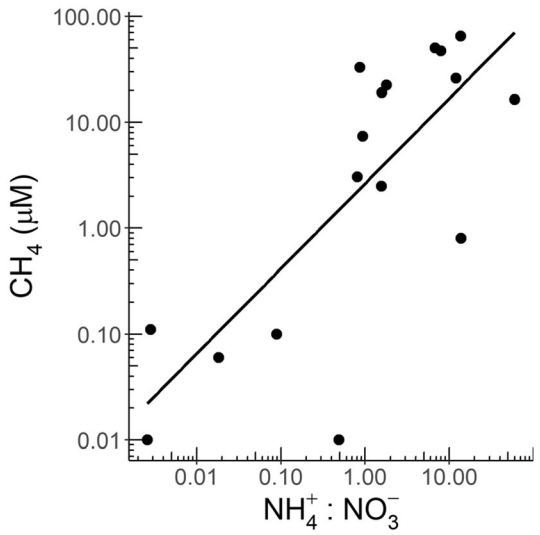

Figure 8. Linear regression between porewater CH_4 concentrations and porewater NH_4/NO_3 ratios (r^2 = 0.59, $p < 0.001$; n_{sites} = 9). Lower ratios indicate a more oxidized environment (more NO_3^-), whereas higher ratios indicate an environment more reduced (more NH_4^+).

ers 2016). Our streams were supersaturated with CH_4 throughout the year (mean supersaturation = 21,280%), consistent with growing evidence that fluvial ecosystems are generally supersaturated and thus sources of CH_4 to the atmosphere (Stanley and others 2016).

Temporal Variability in Stream GHG Concentrations

The temporal variability in concentrations of CO_2, N_2O, and CH_4 provides insight into potential controlling mechanisms across these temperate watersheds. For all three gases, we observed low concentrations in April which we attribute to high flow conditions that either limit the accumulation of dissolved gases or result in outgassing of previously accumulated gases (Dinsmore and others 2013b). Lower concentrations of CO_2 in April may also be due to increased primary productivity relative to respiration given that the only occurrences of supersaturation of DO are in the spring (Figure 4). Winter and summer peaks in dissolved CO_2 occurred during periods of lower flow with maximum concentrations in August when stream temperatures were the highest. These winter and summer peaks are concomitant with periods of high N_2O and CH_4, respectively. Higher N_2O concentrations in winter suggests that this may be a period of increased nitrification, when oxygen levels were near saturation and NH_4^+ concentrations (mean > 70 µg N L^{-1}) were at their peak. In contrast, spikes of N_2O in the summer and fall cooccur with pulses of NO_3^- and occur at times of lower O_2 saturation, which suggests denitrification as the dominant pathway for production of N_2O at these times. Temporal patterns in N_2O concentrations with other metrics of stream chemistry indi-

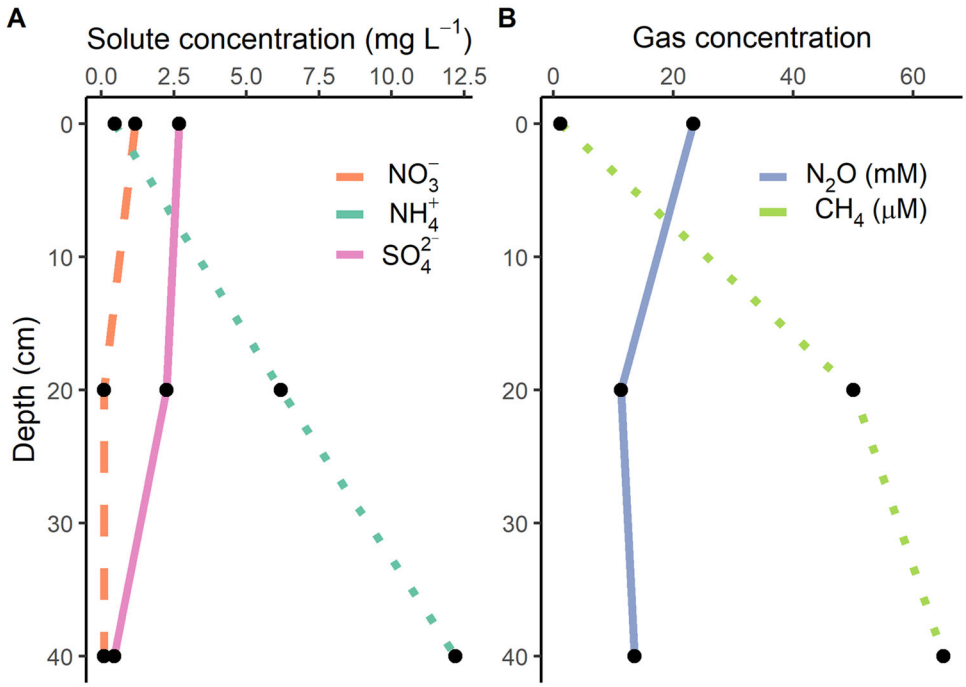

Figure 9. Depth profile of sediment porewater solute (**A**) and dissolved gas (**B**) concentrations at one site (PIK). Samples at depth 0 cm represent surface water samples. Greater depths represent sediment depth at which samples were extracted.

cate that there may be a seasonal switch in the primary N-cycling processes that drive concentrations of N_2O. Variable temporal patterns in N_2O production across sites (Beaulieu and others 2008, 2009; Baulch and others 2011; Audet and others 2017; Borges and others 2018) suggest that drivers and pathways of N_2O production may differ across systems, further complicating management strategies that aim to remove excess N from aquatic ecosystems while avoiding gaseous loss as N_2O (Davis and others 2019).

Methane concentrations were lower during the high flows associated with snow melt (March, April), and higher during low flow periods (summer months), suggesting that CH_4 dynamics may be inversely related to discharge (Stanley and others 2016). In summer months, the combination of low flow, high temperatures and low oxygen availability, along with the depletion of more favorable electron acceptors (NO_3^- and sulfate; SO_4^{2-}) provides conditions suitable for methanogenesis. In August for example, one site (HVH) had particularly high CH_4 concentrations associated with low DO concentrations (43%), likely due to a near-stagnant pool caused by the buildup of debris upstream of our sampling location. Including this site nearly doubles mean CH_4 concentrations for August. Although some previous studies have observed peak CH_4 concentrations in summer and lower concentrations in winter (Dinsmore and others 2013a; Borges and others 2018), others have observed no clear seasonal pattern (Dawson and others 2004). The lack of a consistent seasonal pattern across temperate streams suggests that no single factor, such as discharge, temperature or oxygen availability, is consistently related to CH_4 concentrations (Stanley and others 2016).

Drivers of Stream GHG Concentrations

Both the bivariate and multivariate analyses indicated a unique set of predictor variables for each gas. The strong negative relationship between DO and CO_2, identified through bivariate analysis, is indicative of the tradeoff between respiration and primary production, which may be happening in situ or in the surrounding riparian soils (Figure 4; Borges and others 2015; Hotchkiss and others 2015). The 1:1 line (with a slope of − 1) shown in Figure 4 represents the expected relationship between O_2 and CO_2 if we assume that aerobic metabolism is accounting for most of the measured stream water CO_2 concentrations. Similar to results reported by Crawford and others (2014), our data generally fall to the right of this 1:1 line, indicating that there are additional sources of CO_2 beyond aerobic respiration. This shift indicates the importance of external CO_2 sources (for example, groundwater) in our study streams. However, it is

important to note that forms of anaerobic respiration, such as denitrification or methanogenesis, also contribute to additional production of CO_2, suggesting that respiratory quotients may vary (Crawford and others 2014).

The positive relationship between N_2O and NO_3^- is consistent with many previous studies (for example, Harrison and Matson 2003; Baulch and others 2011; Audet and others 2017), supporting the importance of denitrification as a source of N_2O. Although a positive relationship between NO_3^- and N_2O concentrations is generally attributed to denitrification, it could be interpreted as the accumulation of the products of nitrification (Peterson and others 2001). Thus, future work should investigate the proportion of N_2O concentrations coming from denitrification versus nitrification since management strategies to avoid gaseous loss of N_2O will likely differ depending on the source pathway (Wymore and others 2019).

The unexpected positive relationship between K^+ and N_2O concentrations has, to our knowledge, not been observed in other studies. Although we cannot dismiss the possibility that this correlation is a byproduct of other in-stream processes, collinearity with NO_3^- concentrations (Figure S2), or changing environmental conditions that could influence the concentration of K^+ (for example, pH levels, cation exchange), there are lines of evidence suggesting that K^+ may play an active role in enhancing N_2O production. Potassium was shown to be an effective catalyst in the reduction of NO to N_2O and has been found to increase N reductase enzyme activity in plants; the same family of enzymes involved in catalyzing the sequential steps of denitrification (Khanna-Chopra and others 1980; Kapteijn and others 1984; Víllora and others 2003). Given that our data do not allow us to untangle the mechanism by which K^+ is influencing N_2O concentrations, the relationship between K^+ and N_2O should be interpreted with caution, and we hope future work will provide insight into interactions between K^+ concentrations and N cycling processes.

In contrast to our analyses for CO_2 and N_2O, the variability in CH_4 concentrations across sites was unexplained by any single predictor variable. Although others have found a positive relationship between concentrations of DOC and CH_4, suggesting that C availability drives CH_4 production (Crawford and others 2016; Schade and others 2016), our data show no clear influence of DOC on CH_4 dynamics. We also expected elevated NO_3^- concentrations to inhibit CH_4 production, due to either thermodynamic favorability or toxicity of denitrification byproducts (Bodelier and Steenbergh 2014), but no distinct relationship was observed between NO_3^- and CH_4. Given the contrasting results among various studies, further research is needed to understand the relationship between CH_4 production and NO_3^- concentrations (Crawford and Stanley 2016; Schade and others 2016) as well as to derive predictors of spatial and temporal variability in CH_4 concentrations in streams.

Our multivariate approach using LMM allows us to explore relationships between water chemistry and land use (fixed effects) and gas concentrations, while also accounting for differences among sites (random effect). For all three gases, including site as a random effect improves the variance explained by the LMMs by 26–44% (Table 4). The increase in explained variation for each model, resulting from the inclusion of site as a random effect, indicates that variability in unmeasured site-level characteristics plays an important role in gas responses, a point underscored by the fact that we observed significantly greater spatial variability compared with temporal variability. Characteristics influencing evasion rates, solubility (for example, temperature, conductivity), and connectivity to the surrounding landscape are possible factors influencing site-level variability.

Our results from LMM suggest that the amount of DOC available for respiration influences stream CO_2 concentrations. The negative relationship with DO% shown in both bivariate and multivariate analyses, along with the positive influence of DOC, suggests that CO_2 dynamics are driven by metabolism and terrestrial organic carbon (Table 4; Figure 4) (Cole and others 2007; Borges and others 2015). Our optical DOM data provide evidence of a link between the surrounding terrestrial landscape and stream CO_2 dynamics. Values of FI ranging from 1.2 to 1.5 indicate allochthonous terrestrially sourced DOM, and values between 1.7 and 2.0 indicate autochthonous DOM (McKnight and others 2001). Our small range of FI values falls within the range of allochthonous sources, underscoring a strong landscape influence on CO_2 dynamics, a finding confirmed through our identification of the importance of external inputs to streams in this region (Figure 4).

Geomorphological characteristics are thought to be important drivers of methanogenesis (Stanley and others 2016); however, we found no relationship between sediment characteristics and surface water CH_4 concentrations. The only variables that significantly influenced the LMM for CH_4 were % agriculture (−), % forest (−), and specific conductance (+) (Table 4). Streams draining agri-

cultural landscapes are often associated with elevated concentrations of N and other nutrients (Rabalais 2002). Thus, the negative relationship between % agriculture and CH_4 may be due to the presence of excess nutrients that can inhibit production of CH_4 (Aronson and Helliker 2010). The negative relationship with % forest, in combination with the positive relationship with specific conductance, suggests that as watersheds become more developed, higher amounts of CH_4 can be expected. Other studies have shown that the degree of catchment disturbance (for example, agriculture, urbanization) can be related to the supply of fine sediment due to mechanisms such as soil erosion (Naden and others 2016) and that sediment deposition is a major control of CH_4 production in small streams (Bodmer and others 2020). Similarly, our porewater results highlight the importance of sediment depth in controlling stream CH_4 concentrations at sites with greater sediment deposition.

Porewater as an Indicator of CH_4 Production

Sediment porewater data provide evidence that variability in stream sediments may play an important role in controlling CH_4 production. Our range of surface water to porewater ratios for CH_4 shows that while some sites have higher concentrations in the surface water, many have considerably higher CH_4 concentrations in the deeper sediments (Figure 7). To explore this potential relationship, we developed a depth profile from one of our study sites that shows the influence of redox conditions similar to what we expected to see in the surface water (Figure 9). Moving from the surface water (depth = 0 cm) to the deeper sediments, concentrations of NH_4^+ and CH_4 increase. In contrast, the depth profile also shows a decline in concentrations of NO_3^-, N_2O, and SO_4^{2-} (Figure 9). The concurrent depletion of NO_3^- and N_2O suggests that denitrification becomes limited by NO_3^- availability. Although our sampling technique did not allow for measurements of oxygen at depth, increases in NH_4^+ with concurrent declines in NO_3^- can serve as an indicator of the extent of reducing conditions. This increase in NH_4^+ also suggests that nitrification, another possible source of N_2O, is decreasing with depth. In addition to the porewater depth profile (which could only be explored at one site), CH_4 concentrations were also predicted by porewater NH_4/NO_3 ratios ($r^2 = 0.59$, $p < 0.001$), with increased CH_4 concentrations at higher ratios. The depletion of oxygen and other more thermodynamically favorable terminal electron acceptors (NO_3^- and SO_4^{2-}) with depth appears to create conditions suitable for methanogenesis. We recognize that surface water concentrations may not always reflect the porewater immediately below the point of sampling. Thus, instances of a surface water to porewater ratios greater than one may indicate delivery of CH_4 from an upstream source, such as a wetland or an upstream hyporheic flow path. Nonetheless, we observed that porewater CH_4 concentrations are often much higher than the surface water suggesting that porewater is an important source of CH_4 to the overlying water.

Results from our porewater analysis suggest spatial segregation of biogeochemical processes (for example, denitrification and methanogenesis) due to differences in solute, energy, and oxygen availability between the surface water and varying hyporheic depths (Crawford and Stanley 2016). This could explain why relatively high CH_4 concentrations and fluxes are observed in streams even when inhibitory conditions exist in the surface water (for example, high NO_3^- concentrations), especially considering that there is often high deposition of fine sediments in streams situated within impacted landscapes (Naden and others 2016). These porewater results could also explain the lack of expected predictive relationships with between CH_4 and other surface water measurements.

Greenhouse Gas Production in Stream Environments

We propose a conceptual framework for small streams (Figure 10) in which N_2O production is largely occurring in the surficial sediments, CH_4 production is happening in deep sediments, and CO_2 concentrations are largely due to external sources influenced by the surrounding landscape. Our study identifies the surficial sediments as particularly important to N_2O production, given the relationship of N_2O to metrics of water chemistry (NO_3^-, K^+), corroborating previous work highlighting the importance of benthic-hyporheic N_2O production in small streams (Marzadri and others 2017). In the deeper sediments, CH_4 production becomes more important. The porewater depth profile in combination with the relationship between porewater CH_4 and NH_4/NO_3 ratios confirms that a more reduced environment and depletion of more favorable electron acceptors in the deeper sediments creates hot spots of CH_4 generation. These tight thermodynamic controls observed in the porewater suggest that CH_4 production dominates as we move deeper into the hyporheic zone,

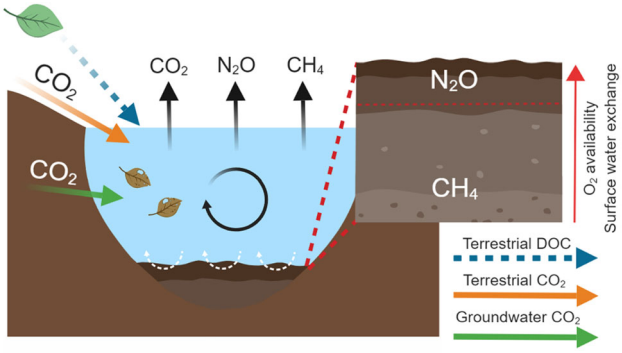

Figure 10. Conceptual framework for greenhouse gas dynamics in small streams. White dashed arrows indicate autochthonous production of CH_4 and N_2O. The black circular arrow represents in-stream processing of DOC and dissolved nutrients. CO_2 concentrations are largely influenced by external inputs, whereas N_2O production dominates in the surficial sediments, and CH_4 production becomes more important in deeper sediments. Created with BioRender.com.

which releases CH_4 to the surface where it can be transported downstream. Contrasting these benthic controls, our results suggest that CO_2 concentrations are largely linked to the surrounding terrestrial landscape and external inputs. Optical DOM data suggest an allochthonous source of DOC, underscoring the role of the surrounding landscape in fueling CO_2 dynamics, as has been suggested in the previous studies (Hotchkiss and others 2015; Campeau and others 2019; Rocher-Ros and others 2019). Future work on stream GHG dynamics can expand this framework to help to disentangle what proportion of measured concentrations result from in-stream processing and external inputs and transport.

ACKNOWLEDGEMENTS

We thank Michelle Shattuck for providing a map of the study sites, Hannah Fazekas for assistance with our modeling approach, and the members of the UNH WQAL for providing feedback on data analysis approaches and assisting with field and lab work. Support for this research was provided by StreamPULSE, NSF Macrosystems Biology 1442444 and the NH Water Resources Research Center. Partial funding was provided by the New Hampshire Agricultural Experiment Station. This work was supported by the USDA National Institute of Food and Agriculture (McIntire-Stennis) Project (1019522). We also acknowledge the efforts of two reviewers whose feedback significantly improved the manuscript.

REFERENCES

Allen GH, Pavelsky TM. 2018. Global extent of rivers and streams. Science 361:585–8.

Aronson EL, Helliker BR. 2010. Methane flux in non-wetland soils in response to nitrogen addition: a meta-analysis. Ecology 91:3242–51.

Audet J, Wallin MB, Kyllmar K, Andersson S, Bishop K. 2017. Nitrous oxide emissions from streams in a Swedish agricultural catchment. Agr Ecosyst Environ 236:295–303.

Barton K. 2019. MuMIn: Multi-Model Inference. R package version 1.43.6. https://CRAN.R-project.org/package=MuMIn.

Bastviken D, Tranvik LJ, Downing JA, Crill PM, Enrich-Prast A. 2011. Freshwater methane emissions offset the continental carbon sink. Science 331:50.

Bates D, Mächler M, Bolker B, Walker S. 2015. Fitting linear mixed-effects models using lme4. J Stat Softw 67:1–48.

Battin TJ, Luyssaert S, Kaplan LA, Aufdenkampe AK, Richter A, Tranvik LJ. 2009. The boundless carbon cycle. Nat Geosci. https://www.nature.com/articles/ngeo618.

Baulch HM, Schiff SL, Maranger R, Dillon PJ. 2011. Nitrogen enrichment and the emission of nitrous oxide from streams. Glob Biogeochem Cycles 25:GB4013.

Beaulieu JJ, Arango CP, Hamilton SK, Tank JL. 2008. The production and emission of nitrous oxide from headwater streams in the Midwestern United States. Glob Change Biol 14:878–94.

Beaulieu JJ, Arango CP, Tank JL. 2009. The effects of season and agriculture on nitrous oxide production in headwater streams. J Environ Qual 38:637–46.

Beaulieu JJ, Tank JL, Hamilton SK, Wollheim WM, Hall RO, Mulholland PJ, Peterson BJ, Ashkenas LR, Cooper LW, Dahm CN, Dodds WK, Grimm NB, Johnson SL, McDowell WH, Poole GC, Valett HM, Arango CP, Bernot MJ, Burgin AJ, Crenshaw CL, Helton AM, Johnson LT, O'Brien JM, Potter JD, Sheibley RW, Sobota DJ, Thomas SM. 2011. Nitrous oxide emission from denitrification in stream and river networks. Proc Natl Sci USA 108:214–19.

Bodelier PL, Steenbergh AK. 2014. Interactions between methane and the nitrogen cycle in light of climate change. Curr Opin Environ Sustain 9–10:26–36.

Bodmer P, Wilkinson J, Lorke A. 2020. Sediment properties drive spatial variability of potential methane production and oxidation in small streams. J Geophys Res Biogeosci 125:e2019JG005213. https://doi.org/10.1029/2019JG005213.

Borges AV, Darchambeau F, Teodoru CR, Marwick TR, Tamooh F, Geeraert N, Omengo FO, Guérin F, Lambert T, Morana C,

Okuku E, Bouillon S. 2015. Globally significant greenhouse-gas emissions from African inland waters. Nat Geosci 8:637–42.

Borges AV, Darchambeau F, Lambert T, Bouillon S, Morana C, Brouyère S, Hakoun V, Jurado A, Tseng H-C, Descy J-P, Roland FAE. 2018. Effects of agricultural land use on fluvial carbon dioxide, methane and nitrous oxide concentrations in a large European river, the Meuse (Belgium). Sci Total Environ 610–611:342–55.

Burgin AJ, Hamilton SK. 2007. Have we overemphasized the role of denitrification in aquatic ecosystems? A review of nitrate removal pathways. Front Ecol Environ 5:89–96.

Campeau A, Bishop K, Amvrosiadi N, Billett MF, Garnett MH, Laudon H, Öquist MG, Wallin MB. 2019. Current forest carbon fixation fuels stream CO2 emissions. Nat Commun 10:1876.

Carrascal LM, Galván I, Gordo O. 2009. Partial least squares regression as an alternative to current regression methods used in ecology. Oikos 118:681–90.

Cole JJ, Prairie YT, Caraco NF, McDowell WH, Tranvik LJ, Striegl RG, Duarte CM, Kortelainen P, Downing JA, Middelburg JJ, Melack J. 2007. Plumbing the global carbon cycle: integrating inland waters into the terrestrial carbon budget. Ecosystems 10:172–85.

Crawford JT, Stanley EH. 2016. Controls on methane concentrations and fluxes in streams draining human-dominated landscapes. Ecol Appl 26:1581–91.

Crawford JT, Striegl RG, Wickland KP, Dornblaser MM, Stanley EH. 2013. Emissions of carbon dioxide and methane from a headwater stream network of interior Alaska. J Geophys Res Biogeosci 118:482–94.

Crawford JT, Lottig NR, Stanley EH, Walker JF, Hanson PC, Finlay JC, Striegl RG. 2014. CO_2 and CH_4 emissions from streams in a lake-rich landscape: patterns, controls, and regional significance. Glob Biogeochem Cycles 28:197–210.

Crawford JT, Loken LC, Stanley EH, Stets EG, Dornblaser MM, Striegl RG. 2016. Basin scale controls on CO2 and CH4 emissions from the Upper Mississippi River. Geophys Res Lett 43:2015GL067599.

Crawford JT, Loken LC, West WE, Crary B, Spawn SA, Gubbins N, Jones SE, Striegl RG, Stanley EH. 2017. Spatial heterogeneity of within-stream methane concentrations. J Geophys Res Biogeosci 122:2016JG003698.

Davis MP, Groh TA, Jaynes DB, Parkin TB, Isenhart TM. 2019. Nitrous oxide emissions from saturated Riparian buffers: are we trading a water quality problem for an air quality problem? J Environ Qual 48:261–9.

Dawson JJC, Billett MF, Hope D, Palmer SM, Deacon CM. 2004. Sources and sinks of aquatic carbon in a peatland stream continuum. Biogeochemistry 70:71–92.

Dinsmore KJ, Billett MF, Dyson KE. 2013a. Temperature and precipitation drive temporal variability in aquatic carbon and GHG concentrations and fluxes in a peatland catchment. Glob Change Biol 19:2133–48.

Dinsmore KJ, Wallin MB, Johnson MS, Billett MF, Bishop K, Pumpanen J, Ojala A. 2013b. Contrasting CO_2 concentration discharge dynamics in headwater streams: a multi-catchment comparison. J Geophys Res Biogeosci 118:445–61.

Drake TW, Raymond PA, Spencer RGM. 2018. Terrestrial carbon inputs to inland waters: a current synthesis of estimates and uncertainty. Limnol Oceanogr Lett 3:132–42.

Harrison J, Matson P. 2003. Patterns and controls of nitrous oxide emissions from waters draining a subtropical agricultural valley. Glob Biogeochem Cycles 17:1–13.

Helms JR, Stubbins A, Ritchie JD, Minor EC, Kieber DJ, Mopper K. 2008. Absorption spectral slopes and slope ratios as indicators of molecular weight, source, and photobleaching of chromophoric dissolved organic matter. Limnol Oceanogr 53:955–69.

Hotchkiss ER, Hall RO Jr, Sponseller RA, Butman D, Klaminder J, Laudon H, Rosvall M, Karlsson J. 2015. Sources of and processes controlling CO_2 emissions change with the size of streams and rivers. Nat Geosci 8:696–9.

Kapteijn F, Mierop AJC, Abbel G, Moulijn JA. 1984. Reduction of NOx over alkali metal–carbon systems. J Chem Soc Chem Commun 0:1085–6.

Keenan TF, Williams CA. 2018. The terrestrial carbon sink. Annu Rev Environ Resour 43:219–43.

Khanna-Chopra R, Chaturverdi GS, Aggarwal PK, Sinha SK. 1980. Effect of potassium on growth and nitrate reductase during water stress and recovery in maize. Physiol Plant 49:495–500.

Lisle TE, Hilton S. 1992. The volume of fine sediment in pools: an Index of sediment supply in gravel-bed streams. J Am Water Resour Assoc 28:371–83.

Marzadri A, Dee MM, Tonina D, Bellin A, Tank JL. 2017. Role of surface and subsurface processes in scaling N2O emissions along riverine networks. Proc Natl Sci USA 114:4330–5.

McKnight DM, Boyer EW, Westerhoff PK, Doran PT, Kulbe T, Andersen DT. 2001. Spectrofluorometric characterization of dissolved organic matter for indication of precursor organic material and aromaticity. Limnol Oceanogr 46:38–48.

Mulholland PJ, Valett HM, Webster JR, Thomas SA, Cooper LW, Hamilton SK, Peterson BJ. 2004. Stream denitrification and total nitrate uptake rates measured using a field 15 N tracer addition approach. Limnol Oceanogr 49:809–20.

Myhre G, Shindell D, Bréon FM, Collins W, Fuglestvedt J, Huang J, Koch D, Lamarque JF, Lee D, Mendoza B, Nakajima T, Robock A, Stephens G, Takemura T, Zhang H. 2013. Anthropogenic and natural radiative forcing. In: Climate Change 2013: The Physical Science Basis. Contribution of Working Group I to the Fifth Assessment Report of the Intergovernmental Panel on Climate Change. Cambridge University Press. pp 659–740.

Naden PS, Murphy JF, Old GH, Newman J, Scarlett P, Harman M, Duerdoth CP, Hawczak A, Pretty JL, Arnold A, Laizé C, Hornby DD, Collins AL, Sear DA, Jones JI. 2016. Understanding the controls on deposited fine sediment in the streams of agricultural catchments. Sci Total Environ 547:366–81. https://doi.org/10.1016/j.scitotenv.2015.12.079.

Nakagawa S, Schielzeth H. 2013. A general and simple method for obtaining R2 from generalized linear mixed-effects models. Methods Ecol Evol 4:133–42.

Noyce GL, Varner RK, Bubier JL, Frolking S. 2014. Effect of *Carex rostrata* on seasonal and interannual variability in peatland methane emissions. J Geophys Res Biogeosci 119:24–34.

Ohno T. 2002. Fluorescence inner-filtering correction for determining the humification index of dissolved organic matter. Environ Sci Technol 36:742–6.

Peterson BJ, Wollheim WM, Mulholland PJ, Webster JR, Meyer JL, Tank JL, Martí E, Bowden WB, Valett HM, Hershey AE, McDowell WH, Dodds WK, Hamilton SK, Gregory S, Morrall

DD. 2001. Control of nitrogen export from watersheds by headwater streams. Science 292:86–90.

Quick AM, Reeder WJ, Farrell TB, Tonina D, Feris KP, Benner SG. 2019. Nitrous oxide from streams and rivers: a review of primary biogeochemical pathways and environmental variables. Earth Sci Rev 191:224–62.

Rabalais NN. 2002. Nitrogen in aquatic ecosystems. Ambio 31:102–12.

Raymond PA, Hartmann J, Lauerwald R, Sobek S, McDonald C, Hoover M, Butman D, Striegl R, Mayorga E, Humborg C, Kortelainen P, Dürr H, Meybeck M, Ciais P, Guth P. 2013. Global carbon dioxide emissions from inland waters. Nature 503:355.

Rocher-Ros G, Sponseller RA, Lidberg W, Mörth C-M, Giesler R. 2019. Landscape process domains drive patterns of CO2 evasion from river networks. Limnol Oceanogr Lett 0.

Romić D, Castrignanò A, Romić M, Buttafuoco G, Kovačić MB, Ondrašek G, Zovko M. 2020. Modelling spatial and temporal variability of water quality from different monitoring stations using mixed effects model theory. Sci Total Environ 704:1–10.

Santos F, Wymore AS, Jackson BK, Sullivan SMP, McDowell WH, Berhe AA. 2019. Fire severity, time since fire, and site-level characteristics influence streamwater chemistry at baseflow conditions in catchments of the Sierra Nevada, California, USA. Fire Ecol 15:3.

Schade JD, Bailio J, McDowell WH. 2016. Greenhouse gas flux from headwater streams in New Hampshire, USA: patterns and drivers. Limnol Oceanogr 61:S165–74.

Smith RE, Kaushal SS, Beaulieu JJ, Pennino MJ, Welty C. 2017. Influence of infrastructure on water quality and greenhouse gas dynamics in urban streams. Biogeosciences 14:2831–49.

Stanley EH, Casson NJ, Christel ST, Crawford JT, Loken LC, Oliver SK. 2016. The ecology of methane in streams and rivers: patterns, controls, and global significance. Ecol Monogr 86:146–71.

Turner PA, Griffis TJ, Baker JM, Lee X, Crawford JT, Loken LC, Venterea RT. 2016. Regional-scale controls on dissolved nitrous oxide in the Upper Mississippi River. Geophys Res Lett 43:2016GL068710.

Team RC. 2019. R: A language and environment for statistical computing. Vienna, Austria: R Foundation for Statistical Computing.

Víllora G, Moreno DA, Romero L. 2003. Potassium supply influences molybdenum, nitrate, and nitrate reductase activity in Eggplant. J Plant Nutr 26:659–69.

Weishaar JL, Aiken GR, Bergamaschi BA, Fram MS, Fujii R, Mopper K. 2003. Evaluation of specific ultraviolet absorbance as an indicator of the chemical composition and reactivity of dissolved organic carbon. Environ Sci Technol 37:4702–8.

Wilcock RJ, Sorrell BK. 2008. Emissions of Greenhouse gases CH4 and N2O from low-gradient streams in agriculturally developed catchments. Water Air Soil Pollut 188:155–70.

Wymore AS, Rodríguez-Cardona BM, Herreid A, McDowell WH. 2019. LINX I and II: lessons learned and emerging questions. Front Environ Sci. https://doi.org/10.3389/fenvs.2019.00181/full.